

DOI: 10.1002/cvde.201106909

Full Paper

Highly Dispersed MoO₃/Al₂O₃ Shell-Core Composites Synthesized by CVD of Mo(CO)₆ under Atmospheric Pressure**

By Guojun Shi, Thomas Franzke, Wei Xia, Miguel D. Sanchez, and Martin Muhler*

MoO₃/γ-Al₂O₃ composites are synthesized by CVD under atmospheric pressure using Mo(CO)₆ as the precursor and porous γ-Al₂O₃ particles in a horizontal, rotating, hot-wall reactor, which is also used for calcination in air. The composites are characterized by N₂ physisorption, atomic absorption spectroscopy, X-ray photoelectron spectroscopy (XPS), X-ray diffraction (XRD), transmission electron microscopy (TEM), and laser Raman spectroscopy (LRS). The synthesized samples exhibit excellent porosity, even at high Mo loadings. A much higher Mo yield is achieved when applying sublimation-adsorption in static air instead of using flowing N₂. A high degree of Mo dispersion on alumina is confirmed by XRD, LRS, and TEM; with a Mo surface density as high as 5.2 atoms nm⁻², the sample is X-ray amorphous, there are no polymeric molybdate species detectable by LRS, and the island size of the molybdate species is about 1 nm according to TEM. The XPS analysis shows that exclusively Mo^{VI} species are present on all synthesized samples. Thus, the applied rotating, hot-wall reactor achieves efficient mixing and homogeneous deposition.

Keywords: Alumina, Molybdenum trioxide, Mo(CO)₆, Rotating hot-wall reactor, Shell-core composites, X-ray photoelectron spectroscopy

1. Introduction

Molybdenum oxides have a rich structural chemistry comprising MoO₃, MoO₂, and numerous shear structures Mo_yO_{3y-1} (y = 4, 5, 8, and 9).^[1] They have received much attention due to their catalytic,^[2] photochromic, and electrochromic properties.^[3,4] MoO₃-based catalysts are applied in the selective oxidation/ammoxidation of propene,^[5,6] the partial oxidation of propane,^[7] the selective oxidation of methane,^[8,9] isomerization of olefins,^[10] and in transesterification reactions.^[11] In heterogeneous catalysis, the catalytic properties depend on the surface and bulk properties of the catalysts, such as the oxidation state of the ions, their local environment, and the type of exposed crystal planes.^[2] The surface properties of supported MoO_x catalysts can be determined by the precursors and preparation methods. In order to realize high yields, a catalyst system has to be prepared that catalyzes the desired main reactions and that eliminates side reactions as much as possible, requiring a thorough control of the surface properties.^[12] The controlled synthesis of heterogeneous

catalysts is a sophisticated art, and numerous efforts have been made to prepare efficiently supported catalysts.^[13] Different synthetic methods are often adopted for the various catalytic reactions to obtain the required surface properties. For example, the surface acidity of catalysts has to be optimized, when MoO₃-based catalysts are used for the isomerization of olefins.^[10] The roles of different exposed crystal planes of crystalline molybdenum trioxide was investigated for the partial oxidation of methane to formaldehyde. It was suggested that the formation of formaldehyde and the total oxidation of methane can be related to the Mo=O sites located on the side plane and the bridging oxygen sites located on the basal planes, respectively.^[14]

Molybdate species can be deposited on supports, such as Al₂O₃, SiO₂, TiO₂, and zeolites. γ-Al₂O₃ is widely used as a support for industrial catalysts due to its outstanding surface and mechanical properties, and its relatively low cost.^[15] As far as catalytic activity is concerned, catalysts with high specific activity and site density should be applied. Impregnation is the usual method for the synthesis of MoO₃/γ-Al₂O₃ catalysts,^[2] however the degree of dispersion of MoO₃ on Al₂O₃ synthesized by impregnation is often inadequate especially at high Mo loadings because of the following three reasons. First, the loading of molybdenum oxide achieved depends on the pore volume of alumina by impregnation. Second, water is often used as the solvent for the Mo precursors, but it is preferentially adsorbed on the surface of alumina, leading to the condensation of the precursor solution and thus a low degree of dispersion.

[*] Dr. G. Shi, Dr. T. Franzke, Dr. W. Xia, Dr. M. D. Sanchez[†]
Prof. M. Muhler
Laboratory of Industrial Chemistry, Ruhr-University Bochum D-44780
Bochum (Germany)
E-mail: muhler@techem.rub.de

[†] Present address: Instituto de Fisica del Sur (UNS-CONICET), 8000
Bahia Blanca (Argentina)

[**] The authors gratefully acknowledge the financial support by the German Research Foundation (DFG, MU 1327/5-1).

Third, the large size of the polyanions, such as $(\text{Mo}_7\text{O}_{24})^{6-}$ and $(\text{Mo}_8\text{O}_{26})^{4-}$, result in slow diffusion rates and poor dispersion of molybdenum oxide on alumina.^[16] Several alternative methods have been developed for the deposition of metal film(s) or particles on oxide supports, among which metal-organic (MO)CVD exhibits attractive properties for the synthesis of supported metal oxide catalysts.^[17,18] In comparison with other methods, MOCVD uses low deposition temperatures and achieves fast growth rates.^[17] Furthermore, the method is not influenced by the pore volume and isoelectric point (IEP) of the substrate, or the solubility of the precursor. A high degree of dispersion can be achieved by CVD due to reaction between the functional groups of the precursor and the substrate forming strong bonds followed by decomposition at elevated temperatures.^[12,19]

Sonnemans and Mars^[20] used two fixed beds to synthesize alumina-supported molybdenum oxide catalysts by CVD. The volatile precursor $\text{MoO}_2(\text{OH})_2$ was generated in the first fixed bed by passing a water/air mixture at 873 K through a bed of MoO_3 particles. The obtained precursor was then fed to another fixed bed packed with alumina. The resulting $\text{MoO}_x/\text{Al}_2\text{O}_3$ catalysts exhibited similar catalytic activities in the dehydrogenation of cyclohexane compared to samples prepared by impregnation with ammonium molybdate.^[20] The application of molybdenum hexacarbonyl and alumina as precursor and support, respectively, to prepare supported catalysts dates back to the work by Banks and Bailey.^[21] They prepared alumina-supported molybdenum carbonyl species by impregnating alumina with a solution of $\text{Mo}(\text{CO})_6$ in cyclohexane at 65 °C. The as-synthesized samples were dried in N_2 and then heated in air.^[21] Other groups directly prepared alumina-supported molybdenum oxide by the CVD of $\text{Mo}(\text{CO})_6$.^[22–24] It was suggested that physically adsorbed $\text{Mo}(\text{CO})_6$ interacts with Lewis acid sites and/or OH groups on the surface of alumina to form complex compounds, which were then decomposed partially or totally at elevated temperatures.

In the present study, we synthesized γ -alumina-supported molybdenum oxide by the CVD of $\text{Mo}(\text{CO})_6$ under atmospheric pressure in a horizontal, rotating, hot-wall reactor. The calcined composites were characterized comprehensively to obtain information on the composition, porosity, phases, degree of dispersion, and on the oxidation

state of the molybdate surface species present on alumina. The aim was to obtain γ -alumina-supported molybdenum oxide catalysts with a high degree of dispersion at high Mo loadings. The $\text{MoO}_3/\text{Al}_2\text{O}_3$ samples are planned to be used as catalysts for the oxidative dehydrogenation of 1-butene and for the selective oxidation of propene.

2. Results and Discussion

γ -alumina-supported molybdenum oxide samples were synthesized by the CVD of $\text{Mo}(\text{CO})_6$ on γ -alumina particles under atmospheric pressure in a horizontal, rotating, hot-wall reactor. The dehydrated γ -alumina particles were thoroughly mixed with $\text{Mo}(\text{CO})_6$, placed in the center of the reactor, and heated to 70 °C in static air. This sublimation temperature was kept constant for 3 h, followed by cooling the reactor. When the reactor temperature had reached 40 °C, a flow of N_2 (80 sccm) and O_2 (20 sccm) was passed through the reactor, and the reactor temperature was increased to 400 °C and kept constant for 180 min to fully calcine the samples. Finally, the samples were cooled to room temperature.

2.1. Surface Properties

Table 1 and Figure 1 present the N_2 physisorption results obtained with the samples. The substrate used in this work was γ -alumina, which exhibited a specific surface area of $167 \text{ m}^2 \text{ g}^{-1}$, a pore volume of 0.26 mL g^{-1} , and a pore diameter of about 4 nm. The specific surface areas and pore volumes decreased with increasing Mo loading, which can be attributed to the relatively low specific surface area of the deposited molybdenum oxide. It can also be clearly seen from the pore size distribution curves (Fig. 1) that the pore diameters slightly decreased after coating MoO_3 on γ -alumina. It is also interesting to note that the pore size distributions of the synthesized samples became more symmetric and narrower compared to the substrate alumina, suggesting that the coated molybdate species on the surface of alumina decorate the exposed defects.^[25]

The decrease in specific surface area due to the deposition of MoO_3 can be analyzed further by assuming that the deposited molybdate species do not contribute to the

Table 1. Specific surface areas and pore volumes of the substrate and the synthesized samples.

Sample ^[a]	$T_{\text{sublimation}}$ [°C]	$T_{\text{decomposition}}$ [°C]	S_{BET} [$\text{m}^2 \text{ g}^{-1}$] ^[b]	pore volume [mL g^{-1}] ^[c]	Mo yield [%]
Al_2O_3	–	–	167	0.26	–
MA-400-4	70	400	155 (147)	0.23	89.7
MA-400-8	70	400	137 (138)	0.21	70.6
MA-400-16	70	400	114 (124)	0.16	65.1

^[a]MA: $\text{MoO}_3/\text{Al}_2\text{O}_3$ prepared by MOCVD;

^[b]The value in parentheses is the specific surface area calculated according to the actual molybdenum loading;

^[c]BJH desorption cumulative pore volume.

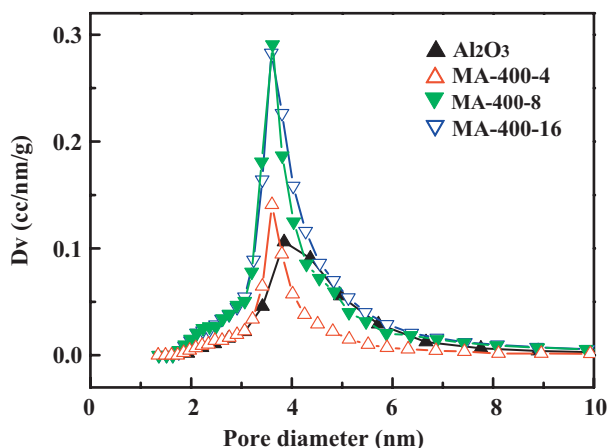


Fig. 1. BJH pore size distribution curves calculated from the nitrogen desorption isotherms of the substrate and the synthesized composites.

specific surface area. Accordingly, the resulting specific surface areas of the synthesized samples taking the actual Mo loading into account are included in parentheses in Table 1. The actual specific surface area of MA-400-4 (7.8 wt.-% Mo) was $8\text{ m}^2\text{ g}^{-1}$ higher than the calculated value, indicating that the deposited molybdate species did not damage the structure of alumina nor block its pores. The sample MA-400-8 (11.5 wt.-% Mo) had a specific surface area in good agreement with the corresponding calculated value. The MA-400-16 (17.1 wt.-% Mo) had a $10\text{ m}^2\text{ g}^{-1}$ lower specific surface area than the calculated value, suggesting that the coated molybdate species led to pore blockage to some extent.

It was found that the yields of the actually deposited molybdate species decreased with increasing Mo loadings (Table 1). Additionally, the sublimation-adsorption of $\text{Mo}(\text{CO})_6$ was also performed in flowing N_2 atmosphere followed by the same post-treatment as MA-400-4. The resulting sample MA-400-4F showed a much lower Mo yield of 29.9% in comparison with MA-400-4 (89.7%), in spite of the same nominal loading and the same deposition temperature. γ -Alumina is a porous material with spinel structure,^[13] and five types of OH groups were found by infrared spectroscopy, which depend on the environment of the aluminum ions in the defective spinel structure.^[26] The total concentration of the OH groups on alumina ranges from 10 to 15 OH nm^{-2} for fully hydroxylated samples, and half of them can be removed at 377 °C. In the present study, alumina was directly used after dehydration at 120 °C, and, correspondingly, the coverage of OH groups was high. In the process of coating $\text{Mo}(\text{CO})_6$ on alumina, gaseous $\text{Mo}(\text{CO})_6$ first physisorbs on alumina, and a complex is formed by the interaction between a surface OH group and a carbonyl ligand of $\text{Mo}(\text{CO})_6$. This process can reversibly proceed by a nucleophilic attack of OH groups followed by the loss of CO and the formation of the complex $\text{Mo}(\text{CO})_{6-x}(\text{OH})$ ($x = 1$ to 5).^[19,24] The resulting complex can easily desorb due to the weak interaction with the support. Accordingly, the yield

was found to be lower in the sample sublimated and adsorbed in flowing N_2 than in the sample prepared in static air, because in flowing N_2 the concentration of gaseous $\text{Mo}(\text{CO})_6$ was lower, favoring the carbonylation reaction and the desorption of the complex.

2.2. XRD Analysis

Figure 2 compares the XRD patterns of samples synthesized at various reaction temperatures and those

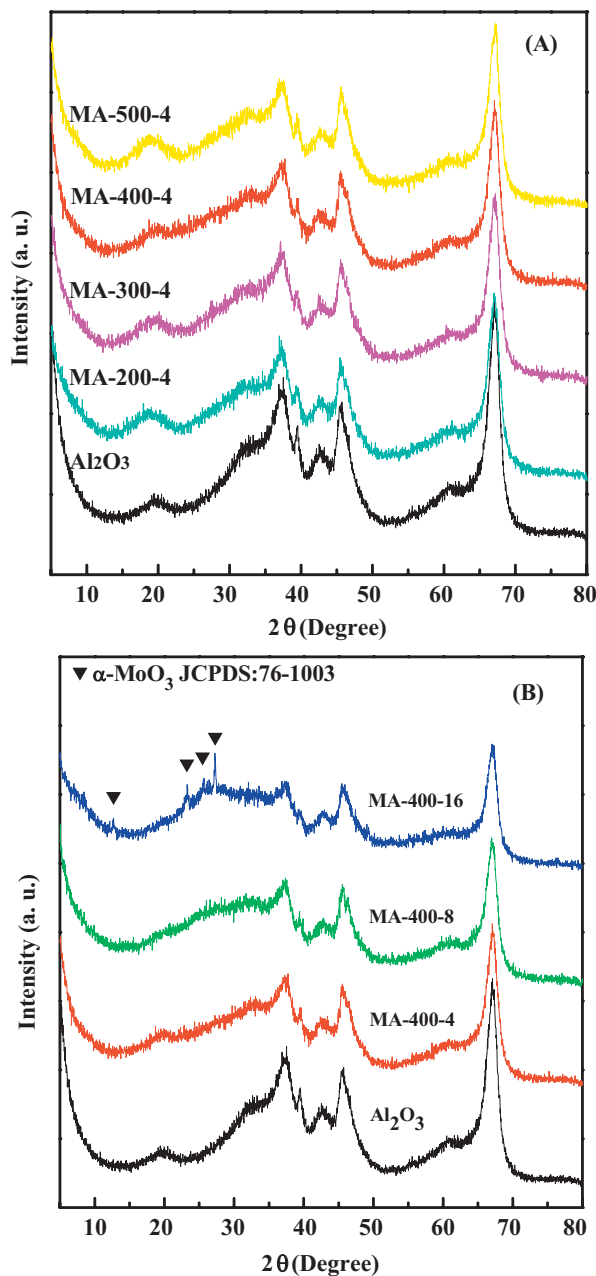


Fig. 2. XRD patterns of samples (A) calcined at various temperatures and (B) with various loadings.

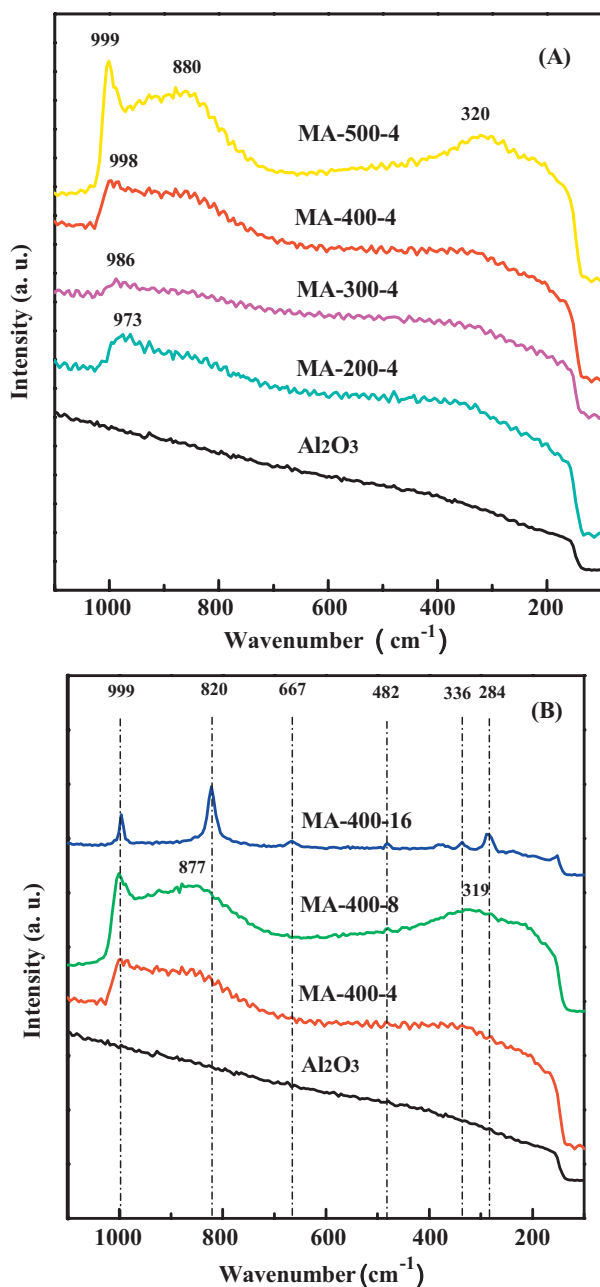


Fig. 3. Raman spectra of samples (A) calcined at various temperatures and (B) with various Mo loadings.

with different loadings. It can be seen from Figure 3A that only the diffraction peaks of γ -alumina were found for all samples with a nominal loading of 4 Mo atoms nm^{-2} prepared at various calcination temperatures. This observation indicates a high degree of Mo dispersion on γ -alumina, even at the high calcination temperature of 500 °C. The weak diffraction peaks of α - MoO_3 were found when the nominal Mo surface density was increased to 16 Mo atoms nm^{-2} . Thus, the XRD analysis indicates that the resulting molybdenum oxide species was α - MoO_3 , which was highly dispersed even at a high Mo loading. The XRD

results are in agreement with the elemental analysis, demonstrating successful Mo coating on γ -alumina, and the N_2 adsorption results confirm the excellent porosity of the composites.

2.3. Laser Raman Spectroscopy

LRS is a sensitive technique for probing the chemical states of molybdate species.^[27] The Raman spectra of alumina-supported molybdenum oxide have been studied extensively. It is generally accepted that the high frequency Raman bands ranging from 840 to 1060 cm^{-1} are related to the terminal Mo=O stretching modes, and that the bands in the regions 200–300 cm^{-1} and 500–800 cm^{-1} are associated with Mo-O-Mo stretching and deformation modes.^[28–38] Figure 3A presents the Raman spectra of samples synthesized at various temperatures. No Raman bands were found for the substrate γ -alumina in the region 100–1100 cm^{-1} . The synthesized samples produced relatively weak fluorescence backgrounds in comparison with γ -alumina. The most prominent peak in all spectra was the strong asymmetric band between 970 and 1000 cm^{-1} . The band shifted from 973 to 999 cm^{-1} and grew in relative intensity when the calcination temperature was increased from 200 to 500 °C. Two new wide bands developed around 880 and 320 cm^{-1} , when the calcination was performed at 400 °C and 500 °C.

The Raman bands at about 990, 880, and 320 cm^{-1} were assigned to the symmetric, asymmetric, and bending stretching modes of the terminal Mo=O bond, respectively.^[28] The asymmetry towards lower wavenumbers of the bands at 973–999 cm^{-1} , and the broadening of the band at 877 cm^{-1} , indicated the presence of different molybdate species strongly interacting with the alumina support.^[37] The band around 990 cm^{-1} shifted towards higher wavenumbers upon increasing the calcination temperature, which could be due to a shorter Mo=O bond and more severe structural distortion.^[28,29] The increase in relative intensity indicated a higher coverage of these molybdate species.

It is important to note that there were no bands originating from the Mo-O-Mo symmetric stretching and Mo-O-Mo deformation modes found in the regions 500–600 cm^{-1} and 200–250 cm^{-1} , respectively.^[28] In addition, there were no bands found around 1006 cm^{-1} and 380 cm^{-1} due to $\text{Al}_2(\text{MoO}_4)_3$. Thus, it can be concluded that the deposited molybdate species on alumina (Fig. 3A) were isolated tetrahedral, octahedral, and other non-polymerized molybdate species indicating a high degree of dispersion on alumina for all samples prepared by MOCVD.

In the case of different loadings (Fig. 3B), the sample MA-400-8 was designed to have two times the Mo loading of the sample MA-400-4, and its bands were at nearly the same positions with slightly higher intensities compared to the sample MA-400-4. Obviously, the polymeric molybdate species were still not detectable for the sample with

the enhanced loading. Sample MA-400-16 with four times the Mo loading of sample MA-400-4 exhibited the well-known bands of crystalline MoO_3 with the characteristic band around 820 cm^{-1} (Fig. 3B). The results indicated that such a high Mo loading resulted in the formation of crystalline MoO_3 , in agreement with the XRD results (Fig. 2B).

2.4. X-ray Photoelectron Spectroscopy

XPS is a surface-sensitive technique widely used for determining the chemical composition of solid surfaces. Several studies applied XPS to investigate the molybdena-alumina system.^[38,40,41] The Al 2p XP spectra of the synthesized samples are shown in Figure 4. For those samples synthesized both at various calcination temperatures (Fig. 4A) and with various loadings (Fig. 4B), the binding energies observed were $\sim 74.3\text{ eV}$, in good agreement with those reported for $\gamma\text{-Al}_2\text{O}_3$.^[42] Additionally, the peak area remained nearly constant for all samples, suggesting that the properties of the alumina support did not change under the experimental conditions.

Figure 5 shows the Mo 3d XP spectra. The Mo 3d doublets (Mo $3d_{3/2}$ and Mo $3d_{5/2}$) were well resolved for all samples, and there was no shift of the binding energy observed for all samples, which agreed well with the Mo 3d binding energy of bulk MoO_3 in the literature.^[42] Thus, the XPS results indicated the presence of only Mo^{VI} species in these samples. Figure 5B presents a corresponding increase in XPS intensity with increasing Mo loading, indicating an increasing Mo coverage.

Figure 6 shows the correlation between the Mo/Al XPS atomic ratio and the calcination temperature (Fig. 6A) and the Mo/Al atomic absorption spectroscopy (AAS) atomic ratio (Fig. 6B). The Mo/Al XPS atomic ratio was found to increase with increasing calcination temperature (Fig. 6A) indicating that the calcination temperature has a beneficial effect on the Mo dispersion on the alumina support. The Mo XPS intensities increased accordingly with the Mo loading (Fig. 6B). A decreasing slope was found when the nominal Mo loading reached 16 Mo atoms nm^{-2} (MA-400-16), which can be attributed to the additional presence of crystalline MoO_3 detected by XRD (Fig. 2B) and LRS (Fig. 3B).

2.5. Transmission Electron Microscopy

Figure 7 presents the TEM images of γ -alumina and the samples synthesized with various Mo loadings. As is seen in Figure 7B, no discrete MoO_3 species were discernible for MA-400-4 with a relatively low Mo loading (7.8%), and its TEM image was similar to that of the pure substrate γ -alumina (Fig. 7A). The diameters of the molybdate islands were estimated to amount to 1 nm and 4 nm for MA-400-8 (11.5 wt.-% Mo) and MA-400-16 (17.1 wt.-% Mo), respectively.

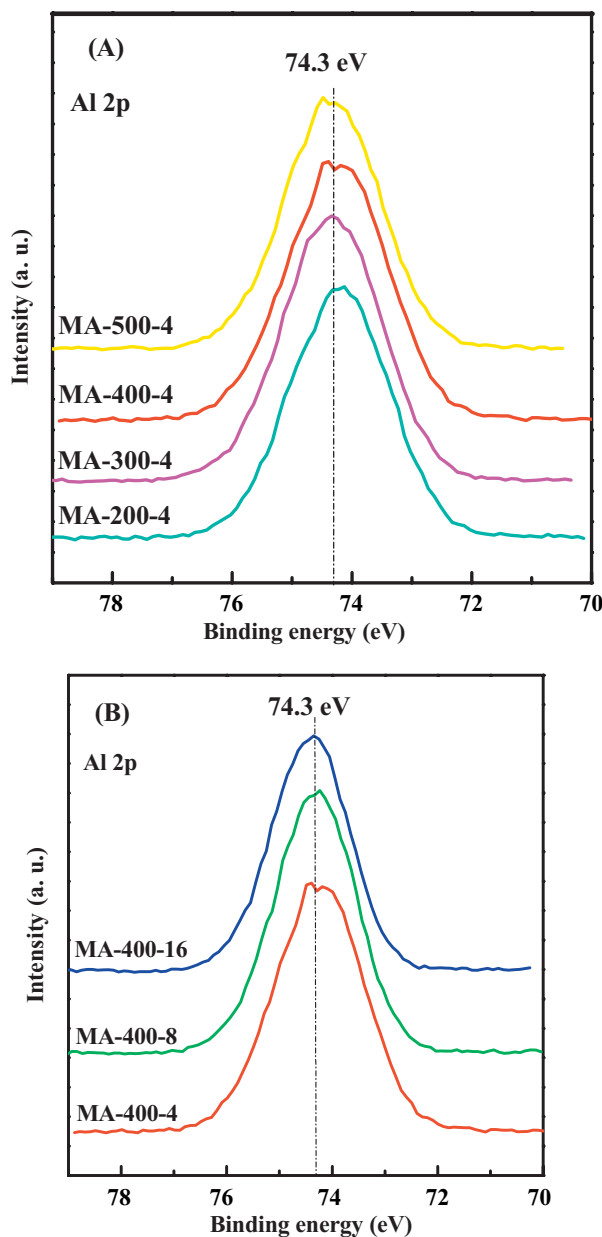


Fig. 4. Al 2p XP spectra of samples (A) calcined at various temperatures and (B) with various Mo loadings.

The XRD analysis excluded the presence of any crystalline phase with large dimensions in samples MA-400-4 and MA-400-8. Combined with their textural properties and the TEM and Raman results, it is assumed that a thin layer of molybdate islands was formed on alumina for samples MA-400-4 and MA-400-8. The former exhibited a higher degree of dispersion due to the relatively low Mo loading, and the molybdate species were not discernible by TEM; the latter yielded an island size around 1 nm and a higher surface density of 5.2 Mo atoms nm^{-2} close to the monolayer surface density reported in the literature (Table 2).^[28] The sample MA-400-16 exhibited weak XRD peaks of $\alpha\text{-MoO}_3$, in

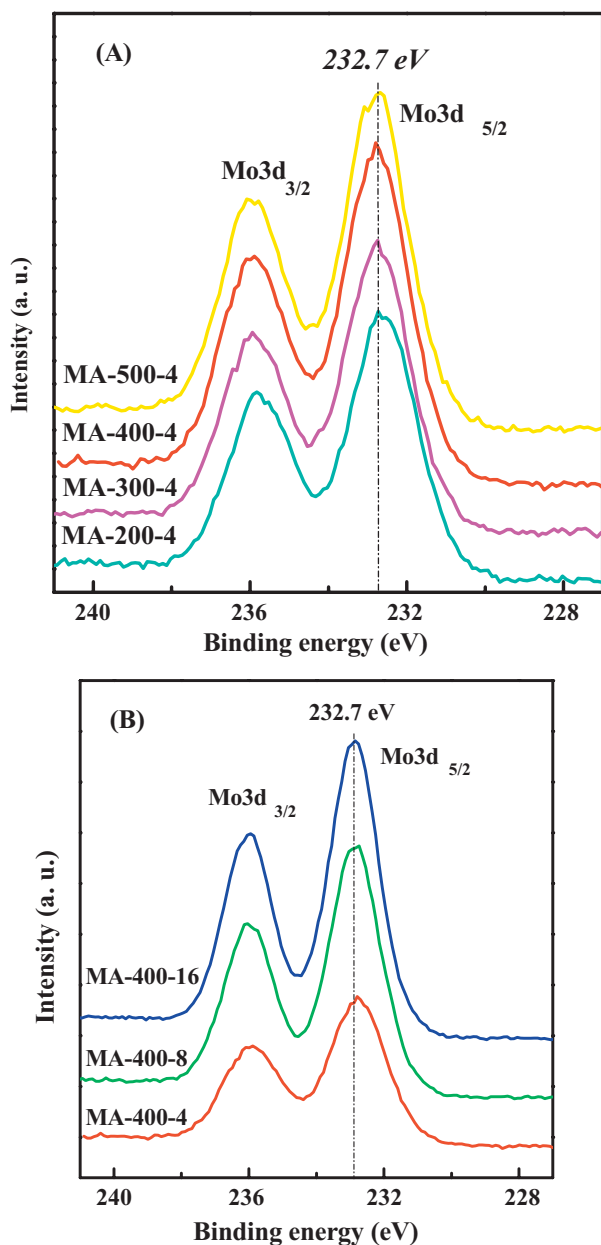


Fig. 5. Mo 3d XP spectra of samples (A) calcined at various temperatures and (B) with various loadings.

agreement with the island size of 4 nm derived from the TEM image.

3. Conclusions

MoO₃/γ-Al₂O₃ catalysts were synthesized by two-step MOCVD under atmospheric pressure with Mo(CO)₆ in a horizontal, rotating, hot-wall reactor. The synthesized samples exhibited excellent porosity at Mo loadings up to 17.1 wt.-%, equivalent to 8.6 Mo atoms nm⁻². The yield of MoO₃ was found to be strongly dependent on the synthesis methods; sublimation-adsorption of the precursor in a static

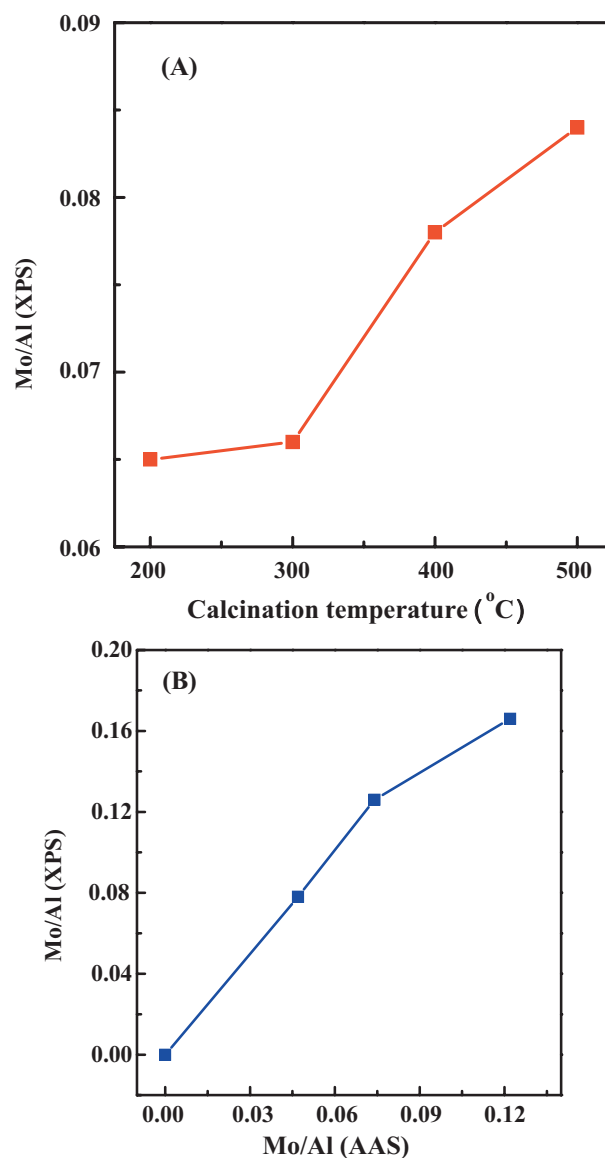


Fig. 6. Mo/Al XPS atomic ratio versus (A) calcination temperature and (B) Mo/Al AAS atomic ratio.

air atmosphere resulted in much higher MoO₃ yields compared to flowing N₂. A high degree of dispersion of the molybdate species was confirmed by XRD, Raman, and TEM studies; at Mo loadings up to 11.5 wt.-%, the samples were X-ray amorphous and contained neither polymeric molybdate species nor Al₂(MoO₄)₃ as detected by LRS, and the molybdate island sizes were about 1 nm according to TEM. The XPS analysis showed that Mo^{VI} is the only Mo species present on all synthesized samples, and that higher calcination temperatures favor the dispersion of molybdate species under the experimental conditions. The steadily increasing Mo/Al XPS atomic ratios with increasing Mo/Al AAS atomic ratio confirmed that the molybdate coverage increased continuously with the Mo loading. The shell-core

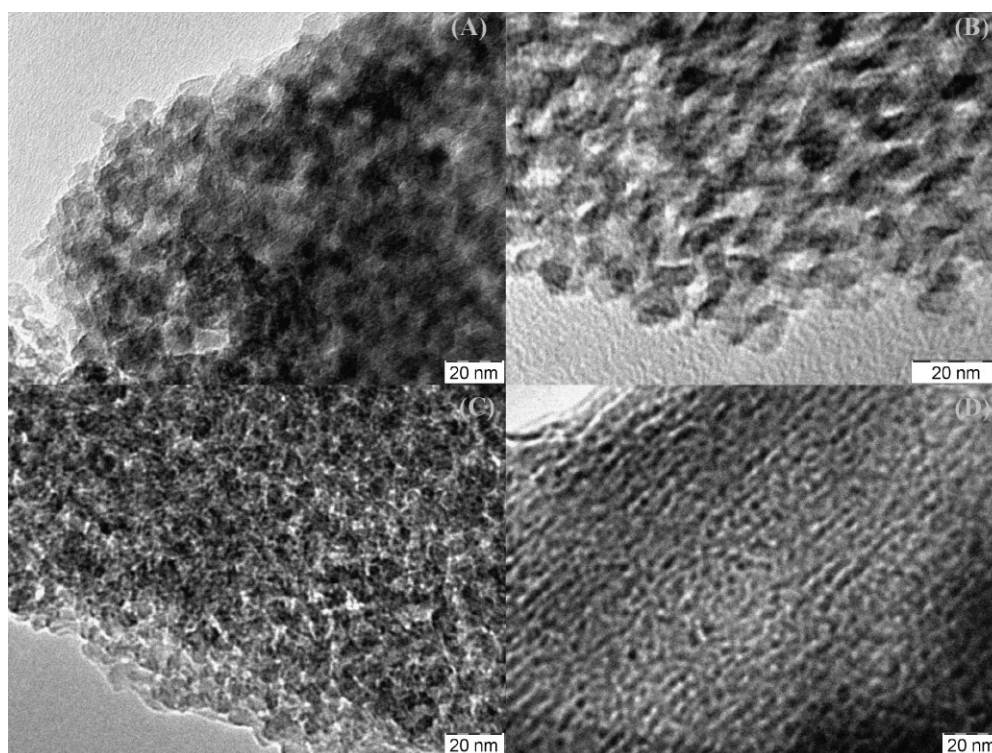


Fig. 7. TEM images of samples calcined at 400 °C with various loadings. (A) γ -Al₂O₃, (B) MA-400-4, (C) MA-400-8, (D) MA-400-16.

Table 2. Surface density of Mo atoms in the synthesized sample.

sample	actual loading [wt.-% Mo]	monolayer surface density ^[a] [Mo atoms nm ⁻²]	actual surface density [Mo atoms nm ⁻²]
MA-400-4	7.8	4.6	3.3
MA-400-8	11.5	4.6	5.2
MA-400-16	17.1	4.6	8.6

^[a]The value is from ref. 28, in which the impregnation method was applied.

composites are considered suitable model catalysts to be applied in selective oxidation reactions.

4. Experimental

γ -Alumina (Fluka, 0.05–0.15 mm) with a specific surface area of 167 m² g⁻¹ was used as the substrate, and the precursor was Mo(CO)₆ (98%, ABCR). CVD was performed under atmospheric pressure in a horizontal, quartz-tube reactor, with a length of 86 cm, and outer and inner diameters of 26 and 21 mm, respectively. A 20 cm long section in the middle of the tube was equipped with 6 mm deep indentations to improve mixing, and a frit (pore size: 10–15 μ m) was positioned at the downstream end of the indented section to prevent discharge. The quartz-tube reactor was placed horizontally in a tubular furnace (Carbolite, length 68 cm, inner diameter 4 cm), with an isothermal zone of more than 30 cm in length, at 400 °C. The quartz-tube reactor was connected to the gas supply equipped with mass flow controllers (MFCs), and the effluent was passed to the ventilation system through a water seal. The reactor was rotated by means of a motor at a rate of about 20 revolutions per minute to achieve efficient mixing and isothermal conditions. The synthesis was divided into two steps; sublimation-adsorption at 70 °C, and oxidative decomposition at elevated temperatures.

In a typical synthesis, 2 g of alumina, which were dehydrated at 120 °C and then cooled down to room temperature in a drier, and 0.60 g (depending on

the loading) of Mo(CO)₆ were thoroughly mixed, and then the mixture was placed in the center of the quartz-tube reactor. The mixture was heated to 70 °C at a ramp of 5 °C min⁻¹, and then this temperature was kept for 3 h in static air or flowing N₂ (for sample MA-400-4F). After the reactor temperature had reached 40 °C, a flow of N₂ (80 sccm) and O₂ (20 sccm) was passed through the reactor. Simultaneously, its temperature was increased at a ramp of 10 °C min⁻¹ to 400 °C and kept for 180 min. Finally, the resulting material was cooled to room temperature in the same atmosphere. The designed loadings of Mo were 4, 8, 16 Mo atoms nm⁻² (γ -alumina), the reaction temperature ranged from 200 to 500 °C, whereas the sublimation temperature was kept constant at 70 °C.

The BET surface area, pore volume, and pore size distribution were determined by static nitrogen physisorption at 77 K (Quantachrome Autosorb-1-MP) after outgassing at 573 K. The pore size distribution was obtained using the BJH method. AAS measurements were performed using a Thermo Electron spectrometer (M-series). Powder XRD patterns were recorded in a Philips X'Pert MPD system with Cu K α radiation. The LR spectra of the synthesized samples were obtained at room temperature in air in a modular system (ALPHA 300R, WITec GmbH). XPS measurements were performed in an ultra-high vacuum set-up equipped with a Gammadata-Scientia SES 2002 analyzer. Monochromatic Al K α (1486.6 eV; 14.5 kV, 45 mA) was used as incident radiation. The spectra were taken at 200 eV pass energy (high pass energy mode) at a base pressure better than 3 \times 10⁻¹⁰ mbar. The obtained binding energies were determined with an overall resolution better than 0.2 eV. Charging effects were compensated by a flood gun. The C 1s binding energy from adventitious hydrocarbon was applied as a charge

reference and fixed at 284.8 eV. The spectrum deconvolution was achieved using the CasaXPS software with Shirley-type background subtraction and with sums of asymmetric Gaussian-Lorentzian functions. The atomic ratios were estimated based on the peak areas, which were corrected with the corresponding atomic sensitivity factors after background subtraction. TEM analysis was carried out using a Hitachi H-8100 transmission electron microscope (200 kV, LaB₆ filament). The samples were prepared by dispersing the powder material in ethanol and dropping the solution on a carbon-coated Au grid.

Received: January 4, 2011

Revised: April 4, 2011

- [1] J. S. Cross, G. L. Schrader, *Thin Solid Films* **1995**, *259*, 5.
- [2] J. Haber, E. Lalik, *Catal. Today* **1997**, *33*, 119.
- [3] T. Ivanova, K. A. Gesheva, P. Sharlandjiev, A. Koserkova-Georgieva, *Surf. Coat. Technol.* **2007**, *201*, 9313.
- [4] J. N. Yao, K. Hashimoto, A. Fujishima, *Nature* **1992**, *355*, 624.
- [5] R. K. Grasselli, J. D. Burrington, *Adv. Catal.* **1981**, *30*, 133.
- [6] Y. Moro-Oka, W. Ueda, *Adv. Catal.* **1994**, *40*, 233.
- [7] J. C. Vedrine, E. K. Novakova, E. G. Derouane, *Catal. Today* **2003**, *81*, 247.
- [8] K. Aoki, M. Ohmae, T. Nanba, K. Takeishi, N. Azuma, A. Ueno, H. Ohfuné, H. Hayashi, Y. Udagawa, *Catal. Today* **1998**, *45*, 29.
- [9] T. Takemoto, K. Tabata, Y. Teng, L.-X. Dai, E. Suzuki, *Catal. Today* **2001**, *71*, 47.
- [10] M. A. Keane, E. C. Alyea, *J. Mol. Catal. A* **1996**, *106*, 277.
- [11] A. V. Biradar, S. B. Umbarkar, M. K. Dongare, *Appl. Catal. A* **2005**, *285*, 190.
- [12] M. Baltés, O. Collart, P. Van Der Voort, F. F. Vansant, *Langmuir* **1999**, *15*, 5841.
- [13] P. Serp, P. Kalck, R. Feurer, *Chem. Rev.* **2002**, *102*, 3085.
- [14] M. R. Smith, U. S. Ozkan, *J. Catal.* **1993**, *141*, 124.
- [15] M. Breyse, P. Afanasiev, C. Geantet, M. Vrinat, *Catal. Today* **2003**, *86*, 5.
- [16] O. Collart, P. Van Der Voort, E. F. Vansant, E. Gustin, A. Bouwen, D. Schoemaker, R. Ramachandra Rao, B. M. Weckhuysen, R. A. Schoonheydt, *Phys. Chem. Chem. Phys.* **1999**, *1*, 4099.
- [17] Q.-H. Wu, M. Gunia, T. Strunskus, G. Witte, M. Muhler, C. Wöll, *Chem. Vap. Deposition* **2005**, *11*, 355.
- [18] W. Xia, Y. Wang, V. Hagen, A. Heel, G. Kasper, U. Patil, A. Devi, M. Muhler, *Chem. Vap. Deposition* **2007**, *13*, 37.
- [19] G. J. Gajda, R. H. Grubbs, W. H. Weinberg, *J. Am. Chem. Soc.* **1987**, *109*, 66.
- [20] J. Sonnemans, P. Mars, *J. Catal.* **1973**, *31*, 209.
- [21] R. L. Banks, G. C. Bailey, *Ind. Eng. Chem. Prod. Res. Dev.* **1964**, *3*, 170.
- [22] T. L. Brown, *J. Mol. Catal.* **1981**, *12*, 41.
- [23] D. C. Bailey, S. H. Langer, *Chem. Rev.* **1981**, *81*, 109.
- [24] K. P. Reddy, T. L. Brown, *J. Am. Chem. Soc.* **1995**, *117*, 2845.
- [25] S. Lim, D. Ciuparu, C. Pak, F. Dobek, Y. Chen, D. Harding, L. Pfefferle, G. Haller, *J. Phys. Chem. B* **2003**, *107*, 11048.
- [26] H. Knözinger, P. Ratnasamy, *Catal. Rev. -Sci. Eng.* **1978**, *17*, 31.
- [27] D. Nicosia, R. Prins, *J. Catal.* **2005**, *234*, 414.
- [28] H. Hu, I. E. Wachs, S. R. Bare, *J. Phys. Chem.* **1995**, *99*, 10897.
- [29] C. C. Williams, J. G. Ekerdt, *J. Phys. Chem.* **1991**, *95*, 8791.
- [30] P. A. Spevack, N. S. McIntyre, *J. Phys. Chem.* **1993**, *97*, 11020.
- [31] M. A. Vuurman, I. E. Wachs, *J. Phys. Chem.* **1992**, *96*, 5008.
- [32] H. Knözinger, H. Jezirowski, *J. Phys. Chem.* **1978**, *82*, 2002.
- [33] H. Hu, I. E. Wachs, *J. Phys. Chem.* **1995**, *99*, 10911.
- [34] X. Gao, Q. Xin, *J. Catal.* **1994**, *146*, 306.
- [35] O. H. Han, C. Y. Lin, N. Sustache, M. McMillan, J. D. Carruthers, K. W. Zilm, G. L. Haller, *Appl. Catal. A* **1993**, *98*, 195.
- [36] H. Jezirowski, H. Knözinger, *J. Phys. Chem.* **1979**, *83*, 1166.
- [37] J. Medema, C. van Stam, V. H. J. de Beer, A. J. A. Konings, D. C. Koningsberger, *J. Catal.* **1978**, *53*, 386.
- [38] D. S. Zingg, L. E. Makovsky, R. E. Tischer, F. R. Brown, D. M. Hercules, *J. Phys. Chem.* **1980**, *84*, 2898.
- [39] A. Bartecki, D. Dembicka, *J. Inorg. Nucl. Chem.* **1967**, *29*, 2907.
- [40] Y. Okamoto, H. Tomloka, Y. Katoh, T. Imanaka, S. Teranishi, *J. Phys. Chem.* **1980**, *84*, 1833.
- [41] B. M. Reddy, B. Chowdhury, E. P. Reddy, A. Fernandez, *Appl. Catal. A* **2001**, *213*, 279.
- [42] J. F. Moulder, W. F. Stickle, P. E. Sobol, K. D. Bomben, *Handbook of X-ray Photoelectron Spectroscopy*, 2nd Ed, Perkin-Elmer Corporation Physical Electronics Division, Minnesota **1992**.